TU Delft

Delft University of Technology

Document Version
Final published version

Licence
Dutch Copyright Act (Article 25fa)

Citation (APA)
van Hattem, A., Vlieland, J., Colineau, E., Griveau, J. C., Konings, R. J. M., & Smith, A. L. (2026). Thermodynamic study of α-$Cs_2Pb(MoO_4)_2$ and safety assessment of the Pb-JOG interaction in lead-cooled fast reactors. *Journal of Nuclear Materials*, *625*, Article 156528. https://doi.org/10.1016/j.jnucmat.2026.156528

Important note
To cite this publication, please use the final published version (if applicable).
Please check the document version above.

Copyright
In case the licence states “Dutch Copyright Act (Article 25fa)”, this publication was made available Green Open Access via the TU Delft Institutional Repository pursuant to Dutch Copyright Act (Article 25fa, the Taverne amendment). This provision does not affect copyright ownership.
Unless copyright is transferred by contract or statute, it remains with the copyright holder.

Sharing and reuse
Other than for strictly personal use, it is not permitted to download, forward or distribute the text or part of it, without the consent of the author(s) and/or copyright holder(s), unless the work is under an open content license such as Creative Commons.

Takedown policy
Please contact us and provide details if you believe this document breaches copyrights.
We will remove access to the work immediately and investigate your claim.

This work is downloaded from Delft University of Technology.

Journal of Nuclear Materials 625 (2026) 156528

Contents lists available at ScienceDirect

Journal of Nuclear Materials

journal homepage: www.elsevier.com/locate/jnucmat

Thermodynamic study of α-$Cs_2Pb(MoO_4)_2$ and safety assessment of the Pb-JOG interaction in lead-cooled fast reactors

Andries van Hattem [a], John Vlieland [a], Eric Colineau [b], Jean-Christophe Griveau [b], Rudy J.M. Konings [a], Anna L. Smith [a,*]

[a] Faculty of Applied Sciences, Radiation Science & Technology Department, Delft University of Technology, Mekelweg 15, Delft, 2629JB, The Netherlands
[b] European Commission, Joint Research Centre (JRC), Karlsruhe, Germany

ARTICLE INFO

Keywords:
JOG
LFRs
PPMS
Solution calorimetry

ABSTRACT

The chemistry following cladding failure in Lead-cooled Fast Reactors involves the interaction between lead (Pb) coolant and the Joint Oxyde Gain (JOG)-phase, mostly composed of dicesium molybdate (Cs_2MoO_4). A thermodynamic analysis of coolant-JOG phase chemical interaction as studied via the scenario of Pb-Cs_2MoO_4 chemical interaction is reported. Measurements of the standard thermodynamic properties of α-$Cs_2Pb(MoO_4)_2$ are presented. The enthalpy of formation of α-$Cs_2Pb(MoO_4)_2$ is measured to be -(2570.7±2.3) kJ·mol^{-1} using solution calorimetry, while the standard entropy is determined to be (399±12) J·K^{-1}·mol^{-1} using thermal-relaxation calorimetry. Thermodynamic calculations show that $Cs_2Pb(MoO_4)_2$ is in several cases thermodynamically stable under conditions typical for operation of Lead-cooled Fast Reactors. This means $Cs_2Pb(MoO_4)_2$ can form in cladding failure scenarios.

1. Introduction

Lead-cooled Fast Reactors (LFRs) are a promising Generation IV nuclear reactor type [1,2]. LFRs use liquid Pb [3,4] or a liquid mixture of Pb and Bi (LBE, lead-bismuth eutectic) [5,6] as primary coolant. In Europe, these fast neutron reactors are envisioned to operate using mixed oxide fuel (MOX), of composition (U,Pu)O_2 with a Pu content up to 30%. The fission product chemistry can be extrapolated from experience with another liquid metal cooled fast reactor type, the Sodium-cooled Fast Reactors (SFRs). Fission products generated with a high fission yield during irradiation and of concern for the safety assessment of the reactor are Cs and Mo [7,8]. Due to their volatile character and the high thermal gradient along the radius of fast reactor fuel pellets, these fission products accumulate in the zone between the fuel pin and the cladding, forming the so-called joint-oxyde-gaine (JOG) phase at high burn-up (above 7–8% FIMA) [7,8]. This is evidenced from post-irradiation examinations [8], while thermodynamic calculations predict the major component of the JOG to be Cs_2MoO_4, besides other phases like Cs_2Te and CsI [9–13]. In the scenario of cladding failure, this JOG-phase can chemically interact with the coolant. To evaluate this scenario for LFRs, it is therefore important to understand the chemistry of the Pb-Cs_2MoO_4 system, and more generally of the Pb-Cs-Mo-O system.

By definition, the Pb-Cs-Mo-O system can be split in its chemical subsystems. A CALPHAD model of the ternary Cs-Mo-O system with corresponding binary Cs-Mo, Cs-O and Mo-O systems has been published by Smith et al. [14], while a CALPHAD model of the ternary Pb-Mo-O system with discussion on the binary Pb-O, Pb-Mo and the same binary Mo-O systems was published by Van Hattem et al. [15]. Moreover, as part of our studies into this system, we have been recently re-investigating the phase diagram Cs_2MoO_4-$PbMoO_4$ [16]. The Cs_2MoO_4-$PbMoO_4$ system has a single compound, $Cs_2Pb(MoO_4)_2$ [16–18], but its thermodynamic properties (enthalpy of formation and standard entropy at 298.15 K) are still unknown.

Herein, experimental data for the standard thermodynamic properties are provided, enabling the application-directed thermodynamic calculations presented thereafter.

2. Methods

2.1. Synthesis and characterisation

$PbMoO_4$ (99.9%) was purchased from Merck Sigma. Cs_2MoO_4 and $Cs_2Pb(MoO_4)_2$ were synthesised by means of solid state reaction and characterised by X-ray diffraction as described in Van Hattem et al. [16].

* Corresponding author.
E-mail address: a.l.smith@tudelft.nl (A.L. Smith).

https://doi.org/10.1016/j.jnucmat.2026.156528
Received 28 July 2025; Received in revised form 4 February 2026; Accepted 9 February 2026
Available online 11 February 2026
0022-3115/© 2026 Published by Elsevier B.V.

The purity was estimated to be higher than 99%. We refer the reader to ref.[16] for more details on the synthesis procedures and detailed characterization. $Cs_2Pb(MoO_4)_2$ shows a palmierite-related monoclinic symmetry ($C2/m$, space group 12), referred to as α-$Cs_2Pb(MoO_4)_2$ up to (626 ± 5) K. Above this temperature, the compound adopts a palmierite structure ($R\bar{3}m$, space group 166), referred to as β-$Cs_2Pb(MoO_4)_2$. The compound melts incongruently (undergoes a peritectic decomposition) at (933 ± 5) K. the transition between α-$Cs_2Pb(MoO_4)_2$ and β-$Cs_2Pb(MoO_4)_2$ was shown to be of second order, with a negligible enthalpy change [16,18,19].

2.2. Low-temperature heat capacity

Low-temperature heat capacity data of a 7.024±0.05 mg α-$Cs_2Pb(MoO_4)_2$ sample was collected with a Quantum Design Physical Property Measurement System (QD-PPMS 14 T) at zero field in the temperature range 2 - 300 K. A thermal connection between the sample and the puck platform was made using Apiezon N-grease. A so-called addenda-curve was measured first, after which the sample was added to the puck with grease and this puck with grease and sample were all measured together. The sample heat capacity equals the difference of the two measurements, a procedure done by the Multiview software of Quantum Design. A 3% uncertainty on the determined heat capacity was used to estimate the error on the heat capacity and standard entropy [20–22].

2.3. Solution calorimetry

A mixture of Cs_2MoO_4 and $PbMoO_4$ was prepared by weighing the compounds in a 1.000:1.000 ratio and grinding for 5 min. The dissolution enthalpies of this mixture and $Cs_2Pb(MoO_4)_2$ in 2 M NaOH were measured using a Precision Solution Calorimeter from TA Instruments with a TAM IV thermostat. The dissolution experiments were performed in a 25 mL Pyrex glass reaction vessel with a golden stirrer holding a glass ampoule. The 1 mL glass ampoule contained about 100 mg sample per measurement and was sealed with wax. Stabilisation of the baseline and calibration before and after the break were performed using an electrical heater. The accuracy of the equipment was assessed by dissolution of KCl (Merck/Supelco pro analysis) in MilliQ water, yielding a value in line with the study of Kilday from the NBS [23].

3. Results and discussion

3.1. Low-temperature heat capacity

The low-temperature heat capacity of α-$Cs_2Pb(MoO_4)_2$ is shown in Fig. 1. The heat capacity does not show any anomaly in the measured temperature window. At room temperature, the heat capacity is close to the value estimated by the Neumann-Kopp rule as applied on Cs_2MoO_4 and $PbMoO_4$ [24,25]. The data has been fitted to a sum of one Debye functions ($D(\Theta_D, T)$) and three Einstein functions ($E(\Theta_E, T)$ in the temperature range 10–298.5 K, which was found sufficient to fit the experimental data. The combined Debye-Einstein formula used for fitting in this work reads thus:

$$C_v(T) = n_D \cdot D(\Theta_D, T) + \sum_{i=1,2,3} n_{E_i} \cdot E(\Theta_{E_i}, T) \quad (1)$$

The classical Dulong-Petit limit should be approached in the sum of $n_D + n_{E_1} + n_{E_2} + n_{E_3}$, while $C_p \approx C_v$ in the fitted temperature range.

Towards the lower limit, the electronic and lattice contributions to the heat capacity are often fitted to a polynomial expression:

$$C_p(T) = \gamma \cdot T + \sum_{n=3,5,7,9} B_n T^n \quad (2)$$

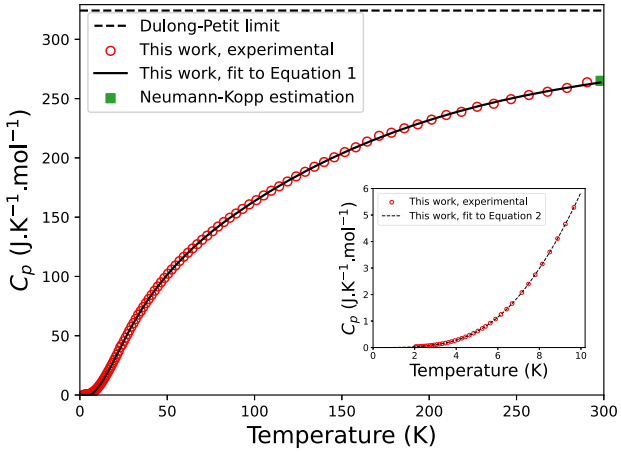


Fig. 1. The heat capacity of α-$Cs_2Pb(MoO_4)_2$ as measured and fitted in this work compared with the values obtained for the Dulong-Petit limit and the Neumann-Kopp approximation. Inset: The fit to the heat capacity of α-$Cs_2Pb(MoO_4)_2$ below 10 K. See for explanation of the fits the main text.

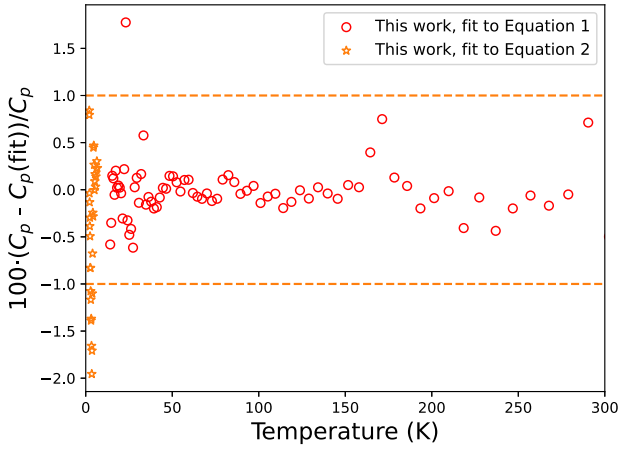


Fig. 2. The difference between the fits as based on the polynomial and the combined Debye-Einstein model and the experimentally determined low temperature heat capacity of α-$Cs_2Pb(MoO_4)_2$. The lines drawn at ±1% are a guide to the eye.

The fit made at the lower temperature limit (T < 10 K) is shown in the inset in Fig. 1, using $\gamma = 0$ mJ·mol^{-1}· K^{-2}. The fitting parameters are given in Table 1. The differences between the fit at low temperature and the combined Debye-Einstein fits (10 < T < 298.15 K) is shown in Fig. 2. As can be seen in the figure, the difference between the fit and experimentally determined data is less than 1%.

In Fig. 3, the heat capacity is plotted in C_p/T vs T to determine the entropy. The shaded area denotes the integrated area. The entropy was both calculated using a linear spline interpolation of the raw data, and an integration of the combined Debye-Einstein model. In both cases, S°_m(298.15 K, α-$Cs_2Pb(MoO_4)_2$,cr) = (399±12) J·K^{-1}·mol^{-1} was obtained, using a total error estimation of 3% on the experimentally determined heat capacity. The heat capacity C_p(298.15 K, α-$Cs_2Pb(MoO_4)_2$, cr) = (264±8) J·K^{-1}·mol^{-1}.

3.2. Solution calorimetry

The measured enthalpies of dissolution of α-$Cs_2Pb(MoO_4)_2$ and the mixture Cs_2MoO_4:$PbMoO_4$ in 2 M NaOH are given in Table 3. The dissolutions were in all cases instantaneous and a minor but significant difference in dissolution enthalpy is observed, meaning the formation of the double molybdate from the two molybdates is slightly exothermic.

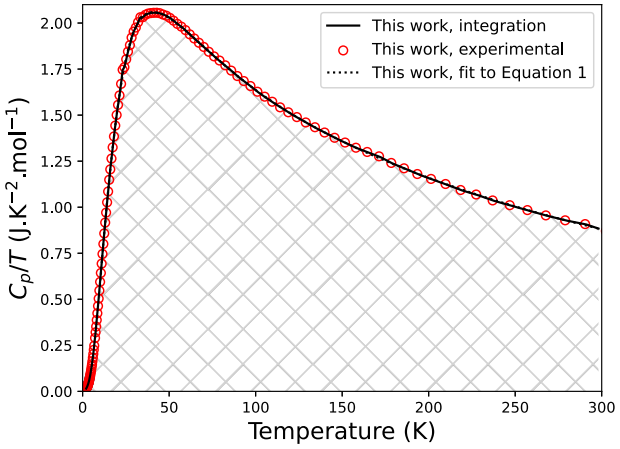


Fig. 3. The low temperature heat capacity of α-$Cs_2Pb(MoO_4)_2$ as plotted in C_p/T vs T to determine the entropy. The dotted line and the full line almost completely overlap.

Table 1
Fitting parameters for the low-temperature heat capacity of α-$Cs_2Pb(MoO_4)_2$.

Temperature range / K	2–10
γ/ J·mol^{-1}· K^{-2}	0
B_3/ J·mol^{-1}· K^{-4}	$3.18 \cdot 10^{-3} \pm 6 \cdot 10^{-5}$
B_5/ J·mol^{-1}· K^{-6}	$8.8 \cdot 10^{-5} \pm 3 \cdot 10^{-6}$
B_7/ J·mol^{-1}· K^{-8}	$-9.5 \cdot 10^{-7} \pm 6 \cdot 10^{-8}$
B_9/ J·mol^{-1}· K^{-10}	$3.3 \cdot 10^{-9} \pm 3 \cdot 10^{-10}$
Temperature range / K	10–298.15
n_D/mol	4.9±0.3
n_{E1}/mol	1.3±0.2
n_{E2}/mol	3.7±0.4
n_{E3}/mol	2.3 ±0.2
Θ_D/K	809 ±35
Θ_{E1}/K	50±10
Θ_{E2}/K	111±5
Θ_{E3}/K	261±32

Using the thermochemical cycle as given in Table 2, the enthalpy of formation from the elements was calculated to be -(2570.7±2.3) kJ·mol^{-1}.

The formation enthalpy, entropy and Gibbs energy at ambient conditions from elements, simple oxides and simple molybdates were calculated using auxiliary literature data and are given in Table 4.

Recent thermodynamic studies on $Cs_2Ba(MoO_4)_2$ [26] and $Cs_3Na(MoO_4)_2$ [27] yielded also Gibbs energies of formation of the complex molybdate from the simple molybdates close to zero (resp. 0.8±4.9 and 2.3±4.2 kJ·mol^{-1}).

4. Margin to formation during LFR operation

In case of cladding failure, the JOG-phase can chemically interact with the coolant and the oxygen dissolved in it. Molybdenum (Mo), that acts in the nuclear fuel as oxygen buffer via the Mo/MoO_2 pair, can be present in multiple oxidation states: as metal Mo(0) in the 5-metal particles, as tetravalent cation Mo(IV) in the perovskite phase ($Ba(Mo,Zr,U)O_3$) or as hexavalent cation Mo(VI) in the scheelite ($Ba(Mo,U)O_4$) or JOG-phase (Cs_2MoO_4). Mo-containing species in the coolant could also originate from structural materials degradation. In the Pb-Mo-O system, three Pb-Mo-O compounds may form [15,33], while there is one Pb-Cs-Mo-O compound known [16]. Here, multiple equilibrium reaction pathways that can be envisaged towards the formation of $PbMoO_4$, Pb_2MoO_5, Pb_5MoO_8 and $Cs_2Pb(MoO_4)_2$ are considered to assess their stability in operating conditions.

4.1. Relation between oxygen potential and oxygen concentration in liquid Pb

First, a relation between the oxygen potential and oxygen concentration in liquid Pb is derived, following a similar procedure as Sreedharan and Gnanamoorthy [34] and Smith et al. [35] took for liquid alkali metals and Müller *et al.* took for liquid Pb and LBE [36,37].

Molecular gases like O_2 dissociate to their atomic counterparts upon dissolution into in liquid metal, known as Sieverts' law [38].

$$\frac{1}{2}O_2 \rightleftharpoons O(Pb) \tag{3}$$

At the oxygen solubility limit in liquid Pb, there is a thermodynamic equilibrium between solid PbO, oxygen dissolved in liquid lead O(Pb) and molecular oxygen (O_2) in the cover gas:

$$Pb(l) + \frac{1}{2}O_2(g) \rightleftharpoons Pb(l) + O(Pb) \rightleftharpoons PbO(s) \tag{4}$$

Equating the first and the last term at equilibrium gives, for a saturation oxygen pressure $p_{O_2,sat}$, and the solvent Pb and solid PbO at unit activity:

$$\Delta_f G^o_m(PbO(s), T) = \frac{1}{2} RT \ln(p_{O_2,sat}) \tag{5}$$

In case of normal operation, the concentration of oxygen dissolved in liquid Pb is below the solubility limit. Below the saturation O(Pb) concentration, the activity of dissolved oxygen is assumed to follow Henry's law and thus to be linear in oxygen (O) concentration:

$$a_O = \gamma_0 c_O = \frac{c_O}{c_{O,sat}} = \sqrt{\frac{p_{O_2}}{p_{O_2,sat}}} \tag{6}$$

This can be rewritten to:

$$p_{O_2,sat} = p_{O_2} \cdot \frac{c^2_{O,sat}}{c^2_O} \tag{7}$$

and combined with Eq. (5) to yield:

$$RT \ln(p_{O_2}) = 2\Delta_f G^o_m(PbO(s)) + 2RT[\ln(c_O) - \ln(c_{O,sat})] \tag{8}$$

Müller et al. [37] give a fit for the saturation concentration of oxygen in Pb, which is based on a data evaluation by Risold et al. [39]:

$$\log c_{O,sat} = 1.64 - \frac{3503}{T} \tag{9}$$

with $c_{O,sat}$ in weight-% and valid in the temperature window $623 < T(K) < 1323$.

Combining Eq. (8) with Eq. (9) yields:

$$RT \ln(p_{O_2}) = 2\Delta_f G^o_m(PbO(s)) + 2RT[\ln(c_{O(Pb)}) - (1.64 - \frac{3503}{T}) \cdot \frac{1}{\log_{10}(e)}] \tag{10}$$

Now, the oxygen potential in liquid Pb versus temperature can be calculated for relevant oxygen concentrations c_O.

4.2. Oxygen potential under operational conditions

Second, knowledge on the typical oxygen concentrations under operational conditions is necessary to answer the question whether the molybdates will form in operational conditions. According to Müller et al. [36], the operational window that prevents PbO precipitation and supports Fe_3O_4 formation as protective oxide scale on the cladding or structural material is defined by:

$$2\Delta_f G^0(PbO) > RT \ln p_{O_2} > \frac{1}{2}\Delta_f G^0(Fe_3O_4) \tag{11}$$

This means that the operational window can be indicated on the diagrams by using the Gibbs energies of formation of PbO [15,39] and Fe_3O_4 [29]. The conditions of Eq. (11) are fulfilled only in the white windows in Fig. 4.

Table 2
Thermochemical cycle used to determine the standard enthalpy of formation of α-$Cs_2Pb(MoO_4)_2$. Measurements performed in the temperature interval T = 298.15±0.2 K. The enthalpy of formation of α-$Cs_2Pb(MoO_4)_2$ was calculated using the relation $\Delta_f H_m^o(5) = \Delta_{sln}H(2) - \Delta_{sln}H(1) + \Delta_f H_m(3) + \Delta_f H_m(4)$. [a] Uncertainty with coverage factor $k=2$ corresponding to a 95% confidence interval. (sln) means 2 M NaOH aqueous solution.

Entry	Reaction	$\Delta_r H$(298.15 K) (kJ·mol^{-1})	ref.
1	α-$Cs_2Pb(MoO_4)_2$(cr) + (sln) = Cs_2MoO_4(sln) + $PbMoO_4$(sln)	24.4±1.5[a]	this work
2	Cs_2MoO_4(cr) + $PbMoO_4$(cr) + (sln) = Cs_2MoO_4(sln) + $PbMoO_4$(sln)	20.8±1.8[a]	this work
3	2Cs(cr) + Mo(cr) + 2O_2(g) = Cs_2MoO_4(cr)	−1514.2±4.3	[14]
4	Pb(cr) + Mo(cr) + 2O_2(g) = $PbMoO_4$(cr)	−1052.9±0.5	[15]
5	2Cs(cr) + Pb(cr) + 2Mo(cr) + 4O_2(g) = α-$Cs_2Pb(MoO_4)_2$(cr)	−2570.7±2.3	this work

Table 3
Measured dissolution enthalpies at 298.15 K in 2 M NaOH for α-$Cs_2Pb(MoO_4)_2$(cr) (M = 792.92 g·mol^{-1}) and the mixture Cs_2MoO_4(cr):$PbMoO_4$(cr). [a] Uncertainty with coverage factor $k=2$ corresponding to a 95% confidence interval.

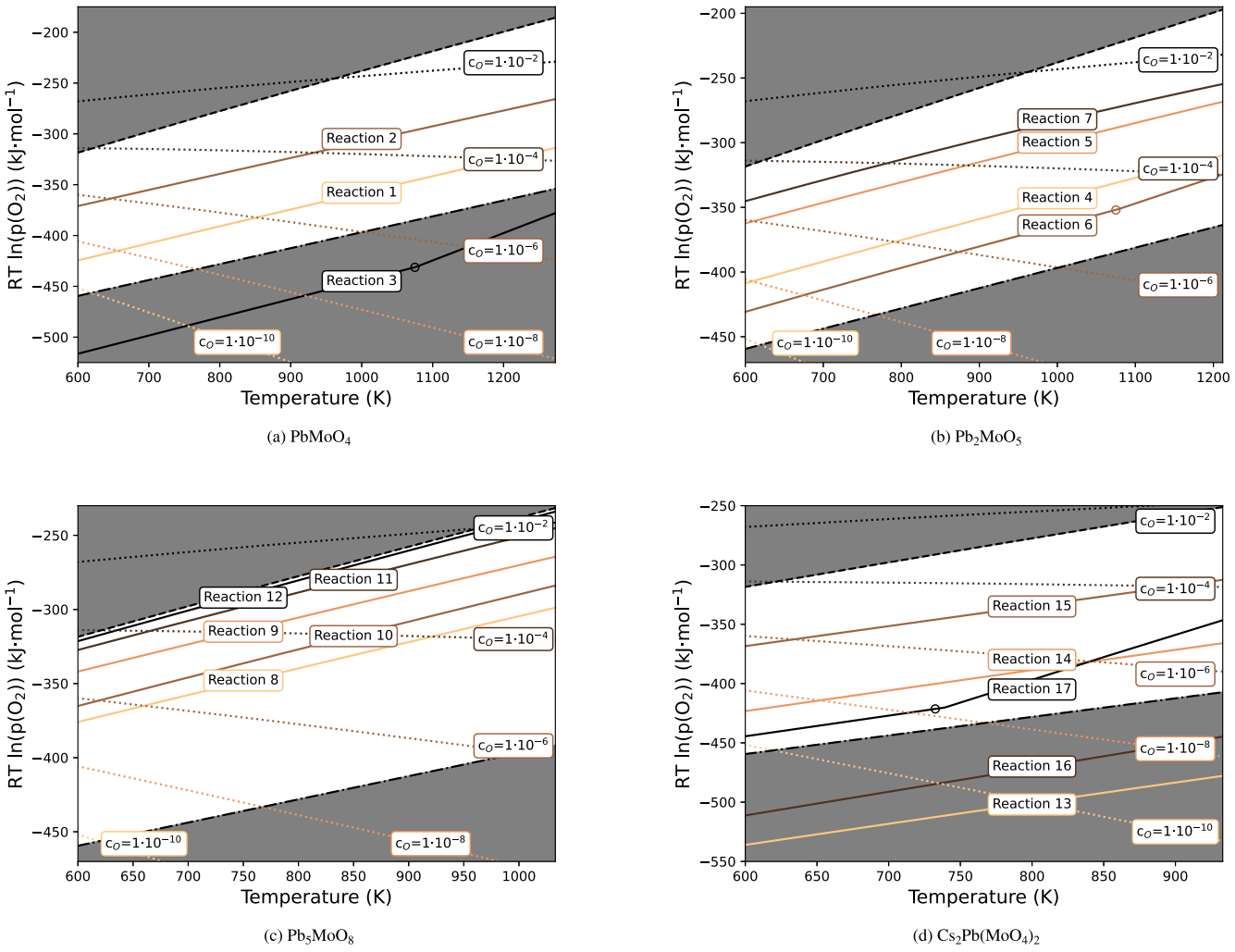
Entry	m($Cs_2Pb(MoO_4)_2$) (mg)	ΔT (mK)	C_p (J·K^{-1})	Q (J)	$\Delta_r H_m^o$(298.15 K) (kJ·mol^{-1})
1	99.30	−26.513	117.381	3.112	24.85
2	99.70	−24.757	117.413	2.907	23.12
3	100.18	−26.938	116.810	3.147	24.92
4	100.57	−26.382	117.916	3.111	24.53
Average					24.4±1.5[a]
Entry	m(Cs_2MoO_4:$PbMoO_4$) (mg)	ΔT (mK)	C_p (J·K^{-1})	Q (J)	$\Delta_r H_m^o$(298.15 K) (kJ·mol^{-1})
1	99.15	−20.838	117.247	2.443	19.54
2	99.77	−24.122	115.514	2.786	22.14
3	100.20	−22.412	117.530	2.634	20.84
4	100.59	−22.385	117.250	2.625	20.69
Average					20.8±1.8[a]

Table 4
Thermodynamic data for α-$Cs_2Pb(MoO_4)$ at ambient conditions. For the elements Cs, Mo and Pb, the S_m° were taken from ref.[28]. The NIST-JANAF tables were used for Mo, PbO and MoO_3 [29], while for Cs_2O values were taken from refs.[30,31] as recommended by Cordfunke and Konings [32]. For Cs_2MoO_4 and $PbMoO_4$, the selected enthalpy and entropy data from Smith et al. and Van Hattem et al. have been used [14,15]. Note that these values may slightly differ from the optimised values used in Fig. 4.

Reaction	$\Delta_r H_m^o$(298.15 K) (kJ·mol^{-1})	$\Delta_r S_m^o$(298.15 K) (J·K^{-1}·mol^{-1})	$\Delta_r G_m^o$ (298.15 K) (kJ·mol^{-1})
2Cs(cr) + Pb(cr) + 2Mo(cr) + 4O_2(g) = α-$Cs_2Pb(MoO_4)_2$(cr)	−2570.7±2.3	−714±12	−2357.8±4.3
Cs_2O(cr) + PbO(cr) + 2MoO_3(cr) = α-$Cs_2Pb(MoO_4)_2$(cr)	−515.0±2.7	30±12	−524.0±4.5
Cs_2MoO_4(cr) + $PbMoO_4$(cr) = α-$Cs_2Pb(MoO_4)_2$(cr)	−3.6±4.9	−10±12	−0.5±6.1

Table 5
Equilibrium reactions and the corresponding Gibbs energy equations for the formation of molybdate compounds in liquid Pb.

Number	Reaction	Gibbs energy equation
1	Pb(l) + Mo(s) + 2O_2(diss) ⇌ $PbMoO_4$(s)	$\Delta\overline{G}_{O_2}^{eq}(T) = RT\ln\frac{P_{O_2}}{p^o} = \frac{1}{2}\Delta_f G_m^o(PbMoO_4(s),T)$
2	Pb(l) + MoO_2(s) + O_2(diss) ⇌ $PbMoO_4$(s)	$\Delta\overline{G}_{O_2}^{eq}(T) = \Delta_f G_m^o(PbMoO_4(s),T) - \Delta_f G_m^o(MoO_2(s),T)$
3	Pb(l) + MoO_3(s,l) + $\frac{1}{2}$$O_2$(diss) ⇌ $PbMoO_4$(s)	$\Delta\overline{G}_{O_2}^{eq}(T) = 2[\Delta_f G_m^o(PbMoO_4(s),T) - \Delta_f G_m^o(MoO_3(s,l),T)]$
4	2Pb(l) + Mo(s) + $\frac{5}{2}$$O_2$(diss) ⇌ Pb_2MoO_5(s)	$\Delta\overline{G}_{O_2}^{eq}(T) = \frac{2}{5}\Delta_f G_m^o(Pb_2MoO_5(s),T)$
5	2Pb(l) + MoO_2(s) + $\frac{3}{2}$$O_2$(diss) ⇌ Pb_2MoO_5(s)	$\Delta\overline{G}_{O_2}^{eq}(T) = \frac{2}{3}[\Delta_f G_m^o(Pb_2MoO_5(s),T) - \Delta_f G_m^o(MoO_2(s),T)]$
6	2Pb(l) + MoO_3(s,l) + O_2(diss) ⇌ Pb_2MoO_5(s)	$\Delta\overline{G}_{O_2}^{eq}(T) = \Delta_f G_m^o(Pb_2MoO_5(s),T) - \Delta_f G_m^o(MoO_3(s,l),T)$
7	2Pb(l) + $PbMoO_4$(s) + $\frac{1}{2}$$O_2$(diss) ⇌ Pb_2MoO_5(s)	$\Delta\overline{G}_{O_2}^{eq}(T) = 2[\Delta_f G_m^o(Pb_2MoO_5(s),T) - \Delta_f G_m^o(PbMoO_4(s),T)]$
8	5Pb(l) + Mo(s) + 4O_2(diss) ⇌ Pb_5MoO_8(s)	$\Delta\overline{G}_{O_2}^{eq}(T) = \frac{1}{4}\Delta_f G_m^o(Pb_5MoO_8(s),T)$
9	5Pb(l) + MoO_2(s) + 3O_2(diss) ⇌ Pb_5MoO_8(s)	$\Delta\overline{G}_{O_2}^{eq}(T) = \frac{1}{3}[\Delta_f G_m^o(Pb_5MoO_8(s),T) - \Delta_f G_m^o(MoO_2(s),T)]$
10	5Pb(l) + MoO_3(s) + $\frac{5}{2}$$O_2$(diss) ⇌ Pb_5MoO_8(s)	$\Delta\overline{G}_{O_2}^{eq}(T) = \frac{2}{5}[\Delta_f G_m^o(Pb_5MoO_8(s),T) - \Delta_f G_m^o(MoO_3(s),T)]$
11	4Pb(l) + $PbMoO_4$(s) + 2O_2(diss) ⇌ Pb_5MoO_8(s)	$\Delta\overline{G}_{O_2}^{eq}(T) = \frac{1}{2}[\Delta_f G_m^o(Pb_5MoO_8(s),T) - \Delta_f G_m^o(PbMoO_4(s),T)]$
12	3Pb(l) + Pb_2MoO_5(s) + $\frac{3}{2}$$O_2$(diss) ⇌ Pb_5MoO_8(s)	$\Delta\overline{G}_{O_2}^{eq}(T) = \frac{2}{3}[\Delta_f G_m^o(Pb_5MoO_8(s),T) - \Delta_f G_m^o(Pb_2MoO_5(s),T)]$
13	Pb(l) + 2Cs(l) + 2Mo(s) + 4O_2(diss) ⇌ $Cs_2Pb(MoO_4)_2$(s)	$\Delta\overline{G}_{O_2}^{eq}(T) = \frac{1}{4}\Delta_f G_m^o(Cs_2Pb(MoO_4)_2(s),T)$
14	Pb(l) + Cs_2MoO_4(s) + Mo(s) + 2O_2(diss) ⇌ $Cs_2Pb(MoO_4)_2$(s)	$\Delta\overline{G}_{O_2}^{eq}(T) = \frac{1}{2}[\Delta_f G_m^o(Cs_2Pb(MoO_4)_2(s),T) - \Delta_f G_m^o(Cs_2MoO_4(s),T)]$
15	Pb(l) + Cs_2MoO_4(s) + MoO_2(s) + O_2(diss) ⇌ $Cs_2Pb(MoO_4)_2$(s)	$\Delta\overline{G}_{O_2}^{eq}(T) = \Delta_f G_m^o(Cs_2Pb(MoO_4)_2(s),T) - \Delta_f G_m^o(Cs_2MoO_4(s) - \Delta_f G_m^o(MoO_2(s),T)$
16	Pb(l) + Cs_2MoO_4(s) + MoO_3(s) + $\frac{1}{2}$$O_2$(diss) ⇌ $Cs_2Pb(MoO_4)_2$(s)	$\Delta\overline{G}_{O_2}^{eq}(T) = 2[\Delta_f G_m^o(Cs_2Pb(MoO_4)_2(s),T) - \Delta_f G_m^o(Cs_2MoO_4(s) - \Delta_f G_m^o(MoO_3(s),T)]$
17	Pb(l) + $Cs_2Mo_2O_7$(s,l) + $\frac{1}{2}$$O_2$(diss) ⇌ $Cs_2Pb(MoO_4)_2$(s)	$\Delta\overline{G}_{O_2}^{eq}(T) = 2[\Delta_f G_m^o(Cs_2Pb(MoO_4)_2(s),T) - \Delta_f G_m^o(Cs_2Mo_2O_7(s,l),T)]$



(a) $PbMoO_4$ (b) Pb_2MoO_5

(c) Pb_5MoO_8 (d) $Cs_2Pb(MoO_4)_2$

Fig. 4. Threshold oxygen potential diagram for the formation of $PbMoO_4$ (a), Pb_2MoO_5 (b), Pb_5MoO_8 (c) and $Cs_2Pb(MoO_4)_2$ (d). The white area indicates a typical operational oxygen potential, were the dashed line corresponds to the formation of PbO and the dashdotted line corresponds to the formation of Fe_3O_4. Oxygen concentrations in wt-% O. See for reactions Table 5 and for explanation the main text. The temperature window is chosen up to the melting point of the respective compounds. The circles in the figures indicate the melting of MoO_3 or $Cs_2Mo_2O_7$.

4.3. Gibbs energy equations

Last, to evaluate which oxygen concentration in liquid Pb is necessary for $PbMoO_4$, Pb_2MoO_5, Pb_5MoO_8 and $Cs_2Pb(MoO_4)_2$ to form, several reactions are written down in Table 5. The corresponding Gibbs energy equations for the formation of complex compounds from coolant, fission products or fission product compounds, and oxygen dissolved in the coolant are written down in Table 5 as well. Gibbs energy functions are taken from Smith et al. [14] and Van Hattem et al. [15] for the Cs-Mo-O and Pb-Mo-O compounds, while the Gibbs energy of $Cs_2Pb(MoO_4)_2$ was calculated by summing the Gibbs energy equations for Cs_2MoO_4 and $PbMoO_4$ and the enthalpy of formation and entropy of formation from molybdates as given in Table 4. Metallic Mo(s) is assumed to have an activity of 1, although its real activity might be lower because it is dissolved in the white 5-metal phase. Cs(l) in reaction 13 is taken equivalent to elemental Cs(l) in the JOG at unit activity.

4.4. Implications for reactor safety

The lower temperature limit of LFR operation is given by the melting point of Pb (600 K). The maximum expected temperature will differ per design and irradiation scheme. By example, for the ALFRED design, the maximum coolant temperature in several transients was calculated to stay always below 1125 K, while the maximum cladding temperature is calculated to be about 1073 K [40]. The temperature range in Fig. 4 starts therefore at 600 K and is limited to the melting point of the compounds or 1273 K.

Within the maximum window for typical operational conditions, the four compounds under study can all form, though not all reaction pathways proposed in Table 5 are possible. $PbMoO_4$ can form from the interaction between liquid Pb, dissolved O and Mo(s) or MoO_2, but not from the reaction of liquid Pb, dissolved O and MoO_3, as can be seen in Fig. 4a. On the other hand, Pb_2MoO_5 can form via all 4 predicted pathways.

Cairang et al. [41] studied oxidation of refractory Mo by liquid lead-bismuth eutectic (LBE) at 873 K with $c_O \approx 2 \cdot 10^{-3}$ wt.-%. They found multilayered oxide scale consisting of MoO_2, $PbMoO_4$ and Pb_2MoO_5. Ignoring the difference between oxygen solubility in liquid Pb and LBE for a second and using Fig. 4a and b, this should be explained by reactions 2 and 7, i.e. a subsequent formation of $PbMoO_4$ and Pb_2MoO_5.

From Fig. 4c, it follows Pb_5MoO_8 formation should be possible, although all reactions are favourable at the high side of the operational window. The slightly lower thermal stability should not hinder its formation at typical coolant temperatures, but its formation may be kinetically hindered.

Whereas the Pb-Mo-O system may be part of the structural materials-coolant interaction, the Pb-Cs-Mo-O system is only relevant in case of cladding failure. Fig. 4d depicts the results for the calculations for the proposed equilibrium reactions towards the formation of $Cs_2Pb(MoO_4)_2$. Reactions 13 and 16 require a too low oxygen concentration to be feasible, whereas reactions 14, 15 and 17 are within the operational window. These reactions start from Cs_2MoO_4 or $Cs_2Mo_2O_7$, phases typically present in the JOG. The melting point of $Cs_2Mo_2O_7$ (732.5 K [14]) is indicated with an open circle on Fig. 4d as well. The presented calculations imply that $Cs_2Pb(MoO_4)_2$ is thermodynamically stable in a cladding failure scenario under typical LFR operational conditions.

5. Conclusions

The enthalpy of formation and standard entropy of α-$Cs_2Pb(MoO_4)_2$ at 298.15 K have been determined experimentally using solution calorimetry and thermal-relaxation calorimetry. $Cs_2Pb(MoO_4)_2$ is thermodynamically stable with respect to its constituting oxides as well as with respect to Cs_2MoO_4 and $PbMoO_4$, though the uncertainty of the Gibbs energy of the latter reaction does not allow a definitive conclusion. However, the result is consistent with the fact that the compound has been synthesised successfully. Thermodynamic calculations have shown that $Cs_2Pb(MoO_4)_2$ as well as $PbMoO_4$, Pb_2MoO_5 and Pb_5MoO_8 are thermodynamically stable under typical operational conditions in a Lead-cooled Fast Reactor.

CRediT authorship contribution statement

Andries van Hattem: Writing – review & editing, Writing – original draft, Visualization, Software, Methodology, Investigation, Formal analysis, Conceptualization; **John Vlieland:** Validation, Investigation, Formal analysis, Data curation; **Eric Colineau:** Validation, Resources, Investigation, Formal analysis, Data curation; **Jean-Christophe Griveau:** Validation, Resources, Investigation, Formal analysis, Data curation; **Rudy J.M. Konings:** Writing – review & editing, Validation, Supervision, Methodology, Conceptualization; **Anna L. Smith:** Writing – review & editing, Validation, Supervision, Resources, Project administration, Methodology, Funding acquisition, Conceptualization.

Data availability

Data will be made available on request.

Declaration of competing interest

The authors declare that they have no known competing financial interests or personal relationships that could have appeared to influence the work reported in this paper.

Acknowledgement

This work has received funding from the Euratom H2020 research project PASCAL (Proof of Augmented Safety Conditions in Advanced Liquid-metal-cooled systems) under grant agreement No. 945341.

The low-temperature heat capacity data reported herein was generated through access to the ActUsLab-PAMEC under the Framework for access to the Joint Research Centre Physical Research Infrastructures of the European Commission (PACIFIED-LFR project, Research Infrastructure Access Agreement No. 36345/01).

Supplementary material

Supplementary material associated with this article can be found in the online version at 10.1016/j.jnucmat.2026.156528

References

[1] C. Fazio, V.P. Sobolev, A. Aerts, S. Gavrilov, K. Lambrinou, P. Schuurmans, A. Gessi, P. Agostini, A. Ciampichetti, L. Martinelli, et al., Handbook on Lead-Bismuth Eutectic Alloy and Lead Properties, Materials Compatibility, Thermal-Hydraulics and Technologies-2015 Edition, Technical Report, Organisation for Economic Co-Operation and Development, 2015.

[2] C.F. Smith, L. Cinotti, Lead-cooled fast reactor, in: Handbook of Generation IV Nuclear Reactors, Elsevier, 2016, pp. 119–155.

[3] A. Alemberti, M. Caramello, M. Frignani, G. Grasso, F. Merli, G. Morresi, M. Tarantino, ALFRED reactor coolant system design, Nucl. Eng. Des. 370 (2020) 110884.

[4] E.O. Adamov, A.V. Kaplienko, V.V. Orlov, V.S. Smirnov, A.V. Lopatkin, V.V. Lemekhov, A.V. Moiseev, BREST Lead-cooled Fast Reactor: from concept to technological implementation, At. Energy 129 (4) (2021) 179–187.

[5] H.A. Abderrahim, P. Kupschus, E. Malambu, P. Benoit, K. Van Tichelen, B. Arien, F. Vermeersch, P. D'hondt, Y. Jongen, S. Ternier, et al., MYRRHA: a multipurpose accelerator driven system for research & development, Nucl. Instrum. Methods Phys. Res., Sect. A 463 (3) (2001) 487–494.

[6] H.A. Abderrahim, P. Baeten, D. De Bruyn, R. Fernandez, MYRRHA–a multi-purpose fast spectrum research reactor, Energy Convers. Manage. 63 (2012) 4–10.

[7] M. Pelletier, Y. Guérin, Fuel performance of fast spectrum oxide fuel, in: R.J.M. Konings, R.E. Stoller (Eds.), Comprehensive Nuclear Materials, 2nd Edition, Elsevier, 2020, pp. 72–105.

[8] F. Cappia, B.D. Miller, J.A. Aguiar, L. He, D.J. Murray, B.J. Frickey, J.D. Stanek, J.M. Harp, Electron microscopy characterization of fast reactor MOX joint oxyde-Gaine (JOG), J. Nucl. Mater. 531 (2020) 151964.

[9] P.A.G. O'Hare, H.R. Hoekstra, Thermochemistry of molybdates I. standard enthalpy of formation of cesium molybdate (Cs_2MoO_4), J. Chem. Thermodyn. 5 (6) (1973) 851–856.

[10] P.A.G. O'Hare, H.R. Hoekstra, Thermochemistry of molybdates V. standard enthalpy of formation of cesium dimolybdate ($Cs_2Mo_2O_7$), J. Chem. Thermodyn. 7 (3) (1975) 279–284.

[11] M. Ugajin, T. Nagasaki, A. Itoh, Contribution to the study of the U-Cs-Mo-I-O system, J. Nucl. Mater. 230 (3) (1996) 195–207.

[12] A.L. Smith, G. Kauric, L. van Eijck, K. Goubitz, G. Wallez, J.-C. Griveau, E. Colineau, N. Clavier, R.J.M. Konings, Structural and thermodynamic study of dicesium molybdate $Cs_2Mo_2O_7$: implications for fast neutron reactors, J. Solid State Chem. 253 (2017) 89–102.

[13] A.L. Smith, J. Vlieland, M.-C. Pignié, M. Abbink, G. Mikaelian, P. Benigni, New insights into the Cs-Mo-O system: experimental studies of the Cs_2MoO_4-MoO_3 pseudo-binary system, Thermochim. Acta 696 (2021) 178825.

[14] A.L. Smith, T.N.P. Thi, C. Guéneau, J.-C. Dumas, E. Epifano, W. van Burik, N. Dupin, Thermodynamic modelling assessment of the ternary system Cs-Mo-O, Calphad 75 (2021) 102350.

[15] A. van Hattem, R. Dankelman, E. Colineau, J.-C. Griveau, K. Dardenne, J. Rothe, S. Couweleers, R.J.M. Konings, A.L. Smith, Experimental investigations and thermodynamic modelling of the ternary system Pb-Mo-O, J. Alloys Compd. 1003 (2024) 175588.

[16] A. van Hattem, J. Vlieland, R. Dankelman, M.A. Thijs, G. Wallez, K. Dardenne, J. Rothe, R.J.M. Konings, A.L. Smith, Structural studies and thermal analysis in the Cs_2MoO_4–$PbMoO_4$ system with elucidation of β-$Cs_2Pb(MoO_4)_2$, Inorg. Chem. 62 (18) (2023) 6981–6992.

[17] G.D. Tsyrenova, Z.G. Bazarova, M.V. Mokhosoev, Double molybdates of cesium and bivalent elements, Dokl. Akad. Nauk SSSR 294 (2) (1987) 387–389.

[18] S.F. Solodovnikov, V.V. Atuchin, Z.A. Solodovnikova, O.Y. Khyzhun, M.I. Danylenko, D.P. Pishchur, P.E. Plyusnin, A.M. Pugachev, T.A. Gavrilova, A.P. Yelisseyev, et al., Synthesis, structural, thermal, and electronic properties of palmierite-related double molybdate α-$Cs_2Pb(MoO_4)_2$, Inorg. Chem. 56 (6) (2017) 3276–3286.

[19] E.F. Dudnik, I.E. Mnushkina, Domain structure and phase transition in $K_2Pb(MoO_4)_2$ single crystals and related compounds, Ukr. J. Phys. 22 (1977) 1737–1738.

[20] J.C. Lashley, M.F. Hundley, A. Migliori, J.L. Sarrao, P.G. Pagliuso, T.W. Darling, M. Jaime, J.C. Cooley, W.L. Hults, L. Morales, et al., Critical examination of heat capacity measurements made on a Quantum Design Physical Property Measurement System, Cryogenics 43 (6) (2003) 369–378.

[21] C.A. Kennedy, M. Stancescu, R.A. Marriott, M.A. White, Recommendations for accurate heat capacity measurements using a Quantum Design Physical Property Measurement System, Cryogenics 47 (2) (2007) 107–112.

[22] P.F. Rosen, B.F. Woodfield, Standard methods for heat capacity measurements on a Quantum Design Physical Property Measurement System, J. Chem. Thermodyn. 141 (2020) 105974.

[23] M.V. Kilday, The enthalpy of solution of SRM 1655 (KCl) in H_2O, J. Res. Natl. Bur. Stand. 85 (6) (1980) 467.

[24] D.W. Osborne, H.E. Flotow, H.R. Hoekstra, Cesium molybdate, Cs_2MoO_4: heat capacity and thermodynamic properties from 5 to 350 K, J. Chem. Thermodyn. 6 (2) (1974) 179–183.

[25] P.M. Aiswarya, R. Ganesan, T. Gnanasekaran, The standard molar enthalpies of formation and heat capacities of $PbMoO_4$(s) and Pb_2MoO_5(s), J. Chem. Thermodyn. 116 (2018) 21–31.

[26] A.L. Smith, N. de Zoete, M. Rutten, L. van Eijck, J.-C. Griveau, E. Colineau, Report of the double-molybdate phase $Cs_2Ba(MoO_4)_2$ with a palmierite structure and its thermodynamic characterization, Inorg. Chem. 59 (18) (2020) 13162–13173.

[27] A.L. Smith, M.-C. Pignié, L. van Eijck, J.-C. Griveau, E. Colineau, R.J.M. Konings, Thermodynamic study of $Cs_3Na(MoO_4)_2$: determination of the standard enthalpy of formation and standard entropy at 298.15 K, J. Chem. Thermodyn. 120 (2018) 205–216.

[28] I. Grenthe, X. Gaona, L. Rao, A. Plyasunov, W. Runde, B. Grambow, R. Konings, A. Smith, E. Moore, M.-E. Ragoussi, et al., Second Update on the Chemical Thermodynamics of Uranium, Neptunium, Plutonium, Americium and Technetium. Chemical Thermodynamics Volume 14, Technical Report, Organisation for Economic Co-Operation and Development, 2020.
[29] M.W. Chase, NIST–JANAF thermochemical tables, J. Phys. Chem. Ref. Data 25 (4) (1996) 1069–1111.
[30] J.L. Settle, G.K. Johnson, W.N. Hubbard, The enthalpy of formation of dicesium monoxide (Cs_2O), J. Chem. Thermodyn. 6 (3) (1974) 263–269.
[31] H.E. Flotow, D.W. Osborne, The heat capacity of dicesium monoxide (Cs_2O) from 5 to 350 K and the Gibbs energy of formation to 763 K, J. Chem. Thermodyn. 6 (2) (1974) 135–140.
[32] E.H.P. Cordfunke, R.J.M. Konings (Eds.), Thermochemical Data for Reactor Materials and Fission Products, Elsevier Science Publishers, 1990.
[33] P.M. Aiswarya, R. Ganesan, T. Gnanasekaran, Partial phase diagrams of Pb-Mo-O system and the standard molar Gibbs energy of formation of $PbMoO_4$ and Pb_2MoO_5, J. Nucl. Mater. 493 (2017) 310–321.
[34] O.M. Sreedharan, J.B. Gnanamoorthy, Oxygen potentials in alkali metals and oxygen distribution coefficients between alkali and structural metals–an assessment, J. Nucl. Mater. 89 (1) (1980) 113–128.
[35] A.L. Smith, C. Gueneau, J.-L. Flèche, S. Chatain, O. Beneš, R.J.M. Konings, Thermodynamic assessment of the Na-O and Na-U-O systems: margin to the safe operation of SFRs, J. Chem. Thermodyn. 114 (2017) 93–115.
[36] G. Müller, G. Schumacher, F. Zimmermann, Investigation on oxygen controlled liquid lead corrosion of surface treated steels, J. Nucl. Mater. 278 (1) (2000) 85–95.
[37] G. Müller, A. Heinzel, G. Schumacher, A. Weisenburger, Control of oxygen concentration in liquid lead and lead–bismuth, J. Nucl. Mater. 321 (2–3) (2003) 256–262.
[38] A. Sieverts, Die Aufnahme von Gasen durch Metalle, Z. für Metallkunde 21 (2) (1929) 37–46.
[39] D. Risold, J.-I. Nagata, R.O. Suzuki, Thermodynamic description of the Pb-O system, J. Phase Equilib. 19 (1998) 213–233.
[40] G. Bandini, E. Bubelis, M. Schikorr, M.H. Stempnievicz, K. Tucek, A. Lázaro, P. Kudinov, K. Kööp, M. Jeltsov, L. Mansani, Safety analysis results of representative DEC accidental transients for the ALFRED reactor, 2013 https://inis.iaea.org/records/rzwaw-87j15
[41] W. Cairang, S. Ma, X. Gong, Y. Zeng, H. Yang, D. Xue, Y. Qin, X. Ding, J. Sun, Oxidation mechanism of refractory molybdenum exposed to oxygen-saturated lead-bismuth eutectic at 600° C, Corros. Sci. 179 (2021) 109132.